Nanocrystalline Calcitic Lens Arrays Fabricated by Self-Assembly Followed by Amorphous-to-Crystalline Phase Transformation

Ingo Schmidt,[†,#] Kyubock Lee,[†,‡,#] Emil Zolotoyabko,[§] Peter Werner,[∥] Tae Soup Shim,[⊥] You-Kwan Oh,[‡] Peter Fratzl,[†] and Wolfgang Wagermaier[†,*]

[†]Department of Biomaterials, Max Planck Institute of Colloids and Interfaces, Potsdam 14424, Germany, [‡]Biomass and Waste Energy Laboratory, Korea Institute of Energy Research, 152 Gajeong-ro, Yuseong-gu, Daejeon 305-343, Korea, [§]Department of Materials Science and Engineering, Technion—Israel Institute of Technology, Haifa 32000, Israel, [∥]Experimental Department II, Max Planck Institute of Microstructure Physics, 06120 Halle, Germany, and [⊥]Department of Chemical and Biomolecular Engineering, KAIST, Daejeon 305-701, Korea. [#]I. Schmidt and K. Lee contributed equally.

ABSTRACT Natural calcium carbonate-based nanocomposites often have superior physical properties and provide a comprehensive source for bioinspired synthetic materials. Here we present thermodynamically stable, transparent $CaCO_3$ microlens arrays (MLA) produced by transforming an amorphous $CaCO_3$ phase into nanocrystalline calcite. We analyze the structure and properties of crystallized MLA by X-ray scattering, transmitted and polarized light microscopy, and electron microscopy and find that MLA are crystallized in spherulite-like patterns without changing the shape of the microlens. The key finding is that nanocrystallinity of the calcite formed diminishes structural anisotropy on the wavelength scale and results in greatly reduced birefringent effects. The remnant preferred orientation of the optical axes of calcite crystals in the plane of the microlens arrays leads to some directionality of optical properties, which may be beneficial for technical applications.

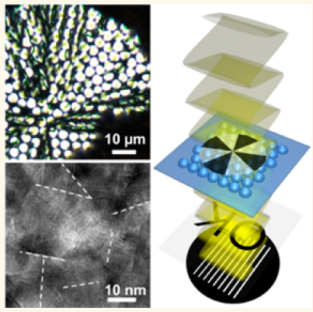

KEYWORDS: biomineralization · crystal growth · X-ray diffraction · optical properties · nanocrystallites

Calcium carbonate is a fundamental building block for many materials in nature,[1−3] and it also attracts growing attention in biomimetic materials research.[4−8] Besides its role as a structural constituent in organisms,[9,10] calcium carbonate also exhibits specific properties enabling, for example, optical functionality.[11,12] The latter is an important feature of some biological materials, being achieved by using complex nanometer-scale architectures.[13] A morphology control of minerals in nature as well as in synthetic materials is possible with the aid of organic macromolecules.[14] In biogenic crystals, macromolecules may guide the nucleation of minerals in a way such that emerging crystals grow with preferential orientation and desired shape.[15,16] Microlenses are one striking example of a functional material made from calcium carbonate.[17] Microlens arrays (MLA) can find technical applications, for example, in directional displays, in artificial compound eyes, or for signal-routing connectors.[18] Strain-responsive MLA have been produced by an elastomer poly(dimethylsiloxane) (PDMS) patterned with a thin layer of hard oxide on top.[19] MLA with integrated pores exhibiting a multipattern photomask were fabricated by lithography techniques.[20]

Here we report on calcitic MLA, produced by a heat-induced transformation from amorphous calcium carbonate (ACC). For long-term applications, it is desirable to transform amorphous materials into the most stable crystalline calcite phase. However, calcite is birefringent, which is potentially unfavorable for optical lenses. Therefore, we explore a way to produce calcium carbonate MLA that meet optical requirements and are thermodynamically stable. For this purpose, we investigated the MLA *in situ* during crystallization by crossed-polarized optical microscopy (POM), microbeam scanning wide-angle X-ray diffraction (WAXD), and transmission electron

* E-mail: wolfgang.wagermaier@mpikg.mpg.de.

Received for review June 3, 2014 and accepted August 12, 2014.

Published online August 12, 2014
10.1021/nn503015c

microscopy (TEM). This allows us to understand the structure and the properties of crystallized MLA and the mechanisms of transformation processes. With the aid of POM we show that amorphous MLA crystallize in spherulite-like patterns without changing the shape of individual hemispherical microlenses. By mapping local crystal orientations, deduced from X-ray diffraction experiments, we find the in-plane distribution of the calcite *c*-axis, as well as calcite twinning of (001) type. We show that the average size of the differently oriented calcite nanocrystals is about 15−20 nm. This fact has a crucial effect on optical characteristics of the crystallized MLA, greatly diminishing the role of the intrinsic birefringence of calcite and preventing undesirable light scattering at grain boundaries.

RESULTS AND DISCUSSION

ACC MLA were prepared according to the previously reported method.[17] The fabricated microlenses had uniform size and focal length. The thin films of ACC MLA, 2−3 μm thick and a few square centimeters in area, can be considered as quasi-two-dimensional, which enabled us to investigate the propagation of crystallization fronts with the aid of POM and WAXD without any sophisticated sample preparation procedures.

Each ACC microlens had a hemispherical shape with a diameter of about 6 μm (Figure 1a). After heat-mediated crystallization, the microlenses still kept their hemispherical shapes (Figure 1b), without using any template at the fabrication and crystallization stages. Other works report unchanged shapes of ACC structures after transformation into calcite by using hard templates.[21−24] We monitored the transformation process *in situ* under a polarized light microscope (Figure 1d−h) by using a temperature-controlled heating stage. The ACC MLA showed predefined cracks (black arrows) induced by the volume change of the fixing polymer (Figure 1c). The transformation of ACC into the crystalline phase at 130−140 °C started with the appearance of a bright spot in the POM image (Figure 1d), which manifested the crystal nucleation event. The crystallization front propagated in radial directions, keeping its circular shape (Figure 1e), and stopped at the predefined cracks, as indicated by white arrows in Figure 1f,g. The ACC phase of MLA had one mole of water per one mole of calcium carbonate, as other typical stable ACC phases had.[17] The new cracks (red arrows, Figure 1h) were generated by volume shrinkage as a result of water release from the ACC phase. In previous studies,[21,25] regularly patterned holes served as sites for the release of water as well as mechanical stresses, and therefore millimeter-sized single crystals of calcite could be formed without cracks.

POM images of crystallized samples look like those produced by spherulites in crystallized polymers, revealing characteristic Maltese crosses (Figure 1e−h). Like the formations of spherulites in polymers, the

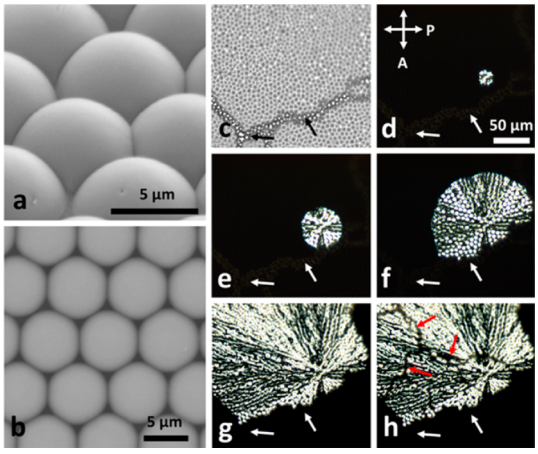

Figure 1. Amorphous-to-crystalline transformation of the $CaCO_3$ microlens array observed by *in situ* light microscopy. SEM image of the homogeneous and well-ordered (a) amorphous and (b) crystallized $CaCO_3$ microlens array. (c) Amorphous microlens array before annealing with predefined cracks (black arrows) induced by the PDMS fixation process. (d−h) Imaging of the transformation process by a crossed-polarized optical microscope: (d) starting time moment, $t = 0$, (e) $t = 5$ s, (f) $t = 14$ s, (g) $t = 24$ s, and (h) $t = 37$ s. Red arrows in (h) mark shrinkage cracks.

centers of Maltese crosses are nucleation sites from which the transformation proceeded in radial directions (Figure 1d−h). These particular POM patterns are greatly influenced by crystal birefringence, as the result of specific orientations of the crystallites formed.

In order to find crystal orientations, we applied microbeam scanning WAXD to selected areas of the samples. Two-dimensional diffraction patterns were taken from calcite crystallites with the aid of a 10 μm sized X-ray beam passing through 3−4 microlenses per sampling point. Figure 2a−d shows orientation maps for different atomic planes (*hkl*), extracted from the X-ray diffraction patterns and superimposed on the respective POM images. A typical diffraction pattern, shown in Figure 2e, reveals segments of Debye rings that manifest a certain degree of preferred orientation. We stress that the maxima of intensity distributions, measured with different reflections (*hkl*), are situated at different azimuthal locations in Figure 2e, the differences being strictly related to the angles between reflecting calcite planes. This circumstance allows us to assume that intensity maxima for different Miller indices (*hkl*) were produced by the same crystallites, which is not trivial when measuring diffraction patterns from polycrystalline samples. By analyzing the orientation map for the (006)-reflection (Figure 2a), we can clearly state that the crystallization front propagates radially from the "point" nucleation event, with the *c*-axis of calcite being the local "crystal growth" direction. Since the angle between the (006)- and (110)-planes is 90°, the orientation map, taken with the (110)-reflection, reveals the expected circular "symmetry" (see Figure 2b). However, when analyzing in this way other

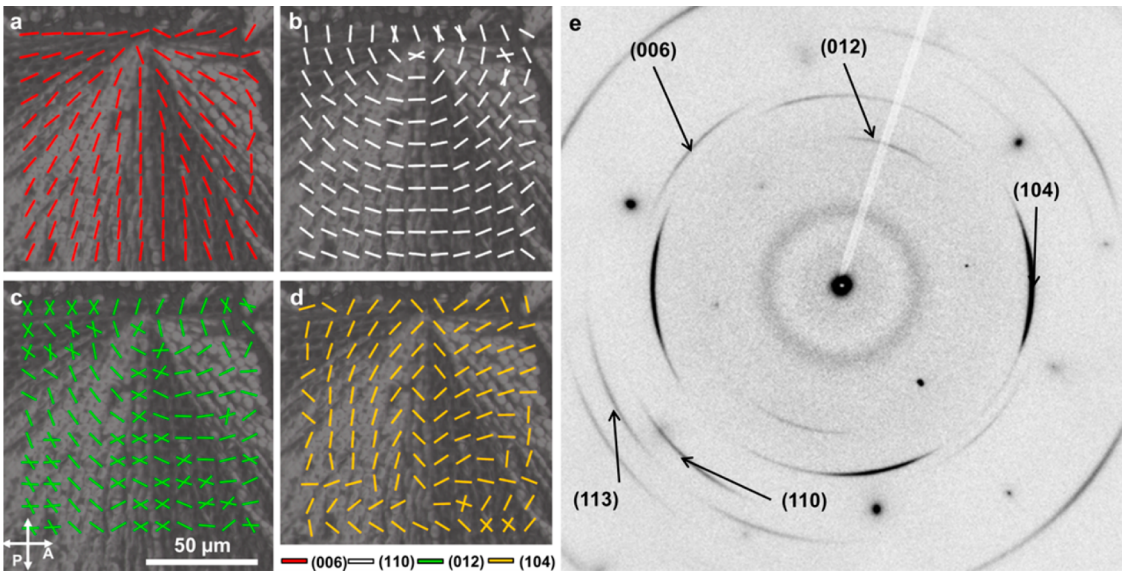

Figure 2. Crystal-orientation maps superimposed on the crossed-polarized optical images. Orientations of different lattice planes are marked by colored bars: (a) (006)-planes (in red), (b) (110)-planes (in white), (c) (012)-planes (in green), and (d) (104)-planes (in yellow). (e) Typical WAXD pattern taken from a calcitic microlens.

available reflections (with enough intensity), we find more complex behavior, shown in Figure 2c and d, for the (012)- and (104)-reflections, respectively. These maps reveal two definite orientations within the same lens or two specific orientations in closely located lenses. Since the angles between these orientation pairs are fixed across the respective images, we assume that these features are induced by twinning in calcite.

Twining in calcite is governed by four twin laws with twin planes of the (001), (104), (012), or (018) type. Atomic arrangements in the vicinity of these twin planes have been described by Pokroy *et al.*[26] Analyzing the orientation maps in Figure 2, we can immediately reject the (104)-, (012)-, and (018)-twinning laws, since they should duplicate crystal orientations in the (006)-map, which does not occur. At the same time, the (001)-twinning law excellently fits all observations. In fact, the (001)-twins do not influence the (006) diffraction intensity (Figure 2a) since atomic rearrangements are within diffractive planes and their projections on the diffraction vector (normal to the diffractive planes) equal zero. Also the (110)-map (Figure 2b) is insensitive to the (001)-twins since Miller index *l*, for diffractive planes, equals zero. So, for observing the twinning effect in the orientation maps we need diffractive planes with a nonzero *l*-index and one or both nonzero *h,k*-indices. These requirements are satisfied when using the (012)- and (104)-reflections. According to Pokroy *et al.*,[26] the expected angles, α, between twinned orientations are $\alpha = 90.8°$ for the (104)-map and $\alpha = 53.8°$ (or 126.2°) for the (012)-map, which fits the observations.

Taking into account the discovered twinning phenomenon, a plausible scenario for an amorphous/crystalline transformation process for ACC MLA looks as follows. Crystallization starts from some nucleation event and proceeds in radial directions, revealing a circular crystallization front. Amorphous/crystalline transformation lowers the bulk free energy, which is in competition with the growing interface energy between the amorphous and the crystalline phase. A circular shape of the crystallization front is thermodynamically favorable since a circle has a minimal border length for a given area surrounded by it. However, radial front propagation from a point source means that adjacent individual crystals, located along slightly misoriented propagation beams, will experience the mismatch strains, contributing to the undesirable elastic energy of the sample. These mismatch strains are removed in the course of plastic deformation, which in our case is provided by the (001)-twinning. Calculations show that the (001)-twin law in calcite has the lowest defect energy, and moreover, only (001)-twins can be generated by a two-dimensional heterogeneous nucleation mechanism.[27] POM images clearly reveal twin boundaries, which separate domains with different crystal orientations, producing lamellar patterns of bright and dark contrast (Figure S1). When the crystalline MLA was tilted by 45° while keeping the same orientation of crossed polarizers, bright domains indicated by orange arrows in the left-hand POM image became dark and *vice versa* (Figure S1).

To understand the relationship between the crystal orientation of MLA and its optical performance as a lens, projection experiments were performed in the partially transformed area of the MLA. This allowed us to compare the optical properties before and after transformation of ACC into calcite (Figures 3, S2, and S3). The POM images clearly show partially crystallized $CaCO_3$ MLA (p-MLA) (Figures 3a and S2). First, we

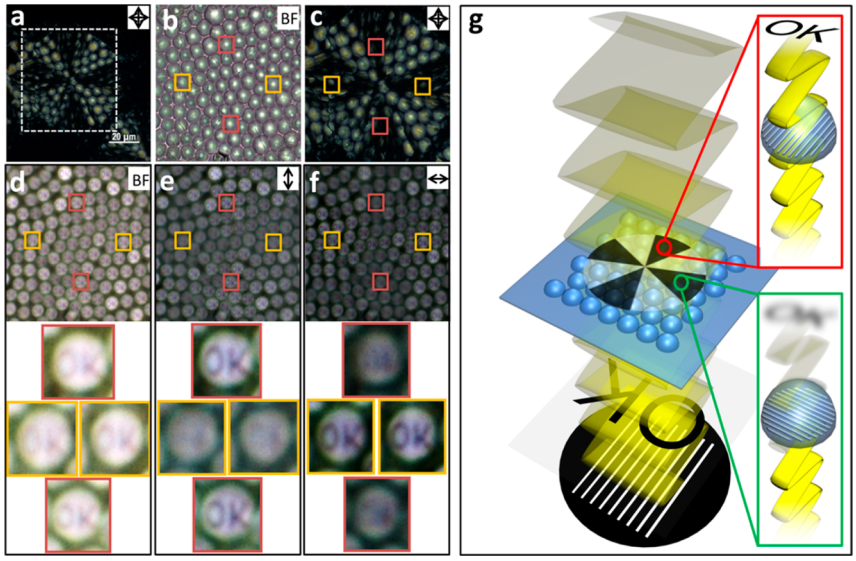

Figure 3. Projection of the "OK" symbol through the MLA sample shown in Figure S3c,d: (a) Optical microscope image taken with crossed polarizers; (b−f) enlarged optical microscope images of white dashed line region shown in (a): (b) bright-field image and (c) image taken with crossed polarizers. The "OK" projection images in the bright field (d) and with polarizers installed in vertical (e) or horizontal (f) orientations; the bottom left panel shows the magnified image indicated by red and yellow boxes in (d), (e), and (f). (g) Schematic illustration of the optical microscope experiment setup and results (red and green boxes): the incident light (color in yellow) passes the optical microscope polarizer, then the glass slide with the "OK" symbol. The fixed p-MLA (colored in blue) produces a Maltese cross that is visible by POM. Inset: Magnified images from sites on the Maltese cross indicated by red and green circles; the lens structure in the red box works as a parallel polarizer, whereas the lens structure in the green box works as a crossed polarizer.

describe the crystal orientation by imaging the "OK" symbol in an optical microscope. All projected "OK"s are visible in the bright-field mode regardless of the crystal orientation in $CaCO_3$ microlenses (see Figure 3d, in which the magnified area, indicated by a white dashed line in Figure 3a, is presented). However, when the light is polarized vertically (in the plane of Figure 3e), the projection images are not visible on the right and left parts of p-MLA (yellow boxes in Figure 3e). When the polarizer was rotated by 90° (horizontal polarization in the plane of Figure 3e), the "OK" projection became visible on the right and left parts of the image, but still remained invisible on the top and bottom parts of p-MLA, indicated by red boxes in Figure 3f. This phenomenon is related to the preferred orientation of the *c*-axis in calcitic MLA (Figure 2a), visualized by the aid of the collected WAXD patterns (Figure 2e). In other words, MLA plays a role of analyzer just as in the standard crossed-polarizer setup (see Figure 3g). More specifically, the linearly polarized light, with a vector of an electric field parallel to the analyzer axis (the *c*-axis of calcite in our case) will be transmitted through the lens array, whereas perpendicularly polarized light will be strongly absorbed.[28] This general optical relationship, together with the *c*-axis orientation maps (Figure 2a), allows us to explain the respective appearance and disappearance of the OK symbol in the corresponding parts of Figure 3e and f.

Second, we observe clear "OK" projection images from both amorphous and crystalline microlenses with preferred orientation, whereas much lower quality projection images are characteristic of randomly crystallized microlenses (Figure S3). It is surprising that the optical properties of calcitic microlenses are comparable to that of amorphous MLA. In fact, crystalline calcite is intrinsically birefringent (resulting in the doubling of optical images) except when light propagates along the optical axis (the *c*-axis), which of course is not the case for polycrystalline MLA.[4,28] In addition, photolithography experiments by using MLA as photomask (randomly crystallized MLA under ambient conditions, except the circular area of p-MLA) confirm the optical transparency of p-MLA (Figure S4).

Based on HR-TEM characterization, we better understand the reasons for the reasonably good optical properties of MLA, which *a priori* could suffer from two drawbacks originating from (i) the polycrystalline character of the lenses and (ii) the birefringence of calcite. In particular, grain boundaries in polycrystalline calcite are the sources of undesirable parasitic light scattering (influencing the lens transparency), whereas birefringence leads to the doubling of optical images. Certainly, the nanocrystalline structure of microlenses (Figure 4a) facilitates a suppression of parasitic scattering from grain boundaries as well as partial averaging and reducing the birefringence effects. Bearing these points in mind, we can say that the nanometer-sized crystallites in our case are so small that the material to some extent loses its optical anisotropy at a scale of the wavelength of visible light. In fact, HR-TEM images clearly show nanocrystallites separated by grain boundaries (white dashed lines in Figure 4a). The average grain

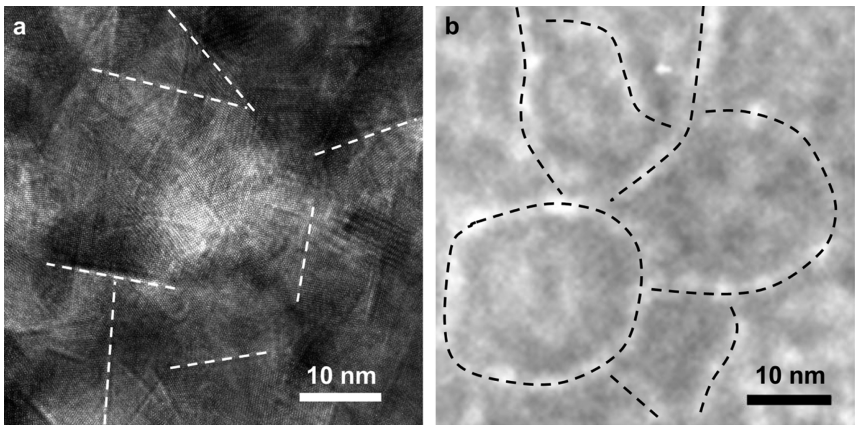

Figure 4. HR-TEM interference and bright-field image of a calcite microlens (a). TEM bright-field image of ACC MLA (b) showing ACC particles surrounded by brighter regions, which are marked by black dashed lines. These regions have lower electron density than the mineral phase and most probably contain water and organic molecules of polysorbate 20, with which the ACC particles are coated.

size (about 15−20 nm) is comparable to that of the initial amorphous particles before crystallization. In fact, TEM bright-field images reveal ACC particles compartmentalized by narrow brighter regions (black dashed lines in Figure 4b), originated in the lower electron density than that in the mineral phase. Most probably, these narrow regions contain water and molecules of surfactant, polysorbate 20, with which the ACC particles are coated.[17] TEM bright-field images, taken under lower magnification (see Figure S5), show clear differences between local spatial inhomogeneities in the amorphous (Figure S5a,b) and crystalline (Figure S5c,d) state. We can speculate that crystallization proceeds by secondary nucleation from one particle to the next.[9,29] When the crystallization front propagates to form preferably oriented crystallites, the organic substance between particles, seemingly, does not allow the secondary nucleation to proceed in a perfectly oriented way.

CONCLUSIONS

In summary, we show how to produce thermodynamically stable MLA, built of nanocrystalline calcite, with greatly diminished birefringence effects and persisting transparency. The calcium carbonate-based MLA described here are morphologically controlled, and the spherical shape of amorphous lenses is preserved after crystallization. The strategy of reducing optical anisotropy in calcitic MLA differs from that found in MLA of brittle stars.[11] Specifically, in brittle stars the optical axes in single crystals of calcite are all parallel to the light propagation direction, the latter being normal to the lens array. This implies that birefringence is absent for this configuration only and will influence the quality of optical images when light deviates from the vertical direction. On the contrary, in our MLA, the optical axes of individual lenses are situated in the horizontal plane, which makes an array much less sensitive to the light propagation direction. In our case, the key issue is the nanocrystallinity of the calcite formed, which reduces the system's anisotropy on the wavelength scale. At the same time, the remaining preferred orientation of the optical axes still provides some directionality of optical properties, which may be beneficial for certain technical applications.

EXPERIMENTAL SECTION

Materials. The $CaCO_3$ MLA were synthesized as described earlier.[17] The MLA can easily be removed from the $Ca(OH)_2$ solution surface and dried at ambient conditions.

Fixation Procedure. The ACC MLA are fixed on a 20 μm mica slide (for X-ray measurements), on glass slides (for POM), or on silicon slides (for TEM) with a thin coating (1 μm) of polydimethylsiloxane.

Crystallization Procedure. A fixed ACC MLA can easily be crystallized by heat treatment for 1 h at 300 °C. The *in situ* heating experiments were performed with a Linkam THMS600 heating stage. To obtain p-MLA, thermal treatment of ACC MLA fixed on glass slides was carried out on a hot plate at 200 °C for 30 s followed by quick cooling and removing the MLA from the plate.

Polarization Optical Microscopy. The circular crystallized area of p-MLA was imaged with an optical microscope (Microscope Axio ImagerA2, Carl Zeiss Microscopy GmbH) using crossed polarizers (Figure S2a). A polycrystalline region with random orientation was observed around the circular area of p-MLA after the sample was left in air for 3 days (Figure S2c−e). The ACC phase was crystallized under ambient conditions. The initial weak crystallinity is better revealed when both polarizer and analyzer are aligned in parallel, than under crossed polarization (Figure S2). The projection imaging was performed with the setup shown in Figure S3g. The bright-field projection images were obtained with no polarizer and analyzer (Figure 3d) or with only a polarizer installed (in vertical or horizontal orientation, Figure 3e,f, respectively). Overview POM images of completely crystallized MLA samples used for X-ray measurements were obtained by using a Leica DM RXA2 and treated with a digital color camera, Leica DFC 480.

X-ray Measurements. Microbeam wide-angle X-ray diffraction experiments were performed at the μSpot beamline of the synchrotron radiation source (BESSY II). The incident X-ray beam (wavelength, λ = 0.82656 Å) was focused horizontally and

vertically down to a 10 μm spot, with the aid of a toroidal mirror, followed by a MoBC-multilayer monochromator.[30] A two-dimensional CCD-based MAR mosaic detector was used to record the diffraction patterns (measurement range in q-space: 0.3–28 nm^{-1}).[30] In order to obtain the spatially resolved structural information, 10 μm steps in the sample scanning mode were applied. The calibrations of the sample-to-detector distance and beam center were carried out by using the software Fit2d (by Andy Hammersley, ESRF, v. 12.077). The data evaluation was performed by using the software packages DPDAK (DESY/MPIKG, Gunthard Benecke, v. 0.3.0. beta2) and OriginPro.

TEM Measurements. ACC and crystalline MLA fixed on TEM sample holders were coated with a thin platinum layer using e-beam deposition and then cut by focused ion-beam (FIB). The images were obtained by the aid of a FEI TITAN 80-300 instrument operated at 300 keV.

Conflict of Interest: The authors declare no competing financial interest.

Acknowledgment. Ingo Schmidt and Kyubock Lee contributed equally to this work. We thank C. Li, S. Siegel, and C. Pilz (MPI of Colloids and Interfaces, Potsdam) for technical assistance and H. Blumtritt (MPI of Microstructure Physics, Halle) for the preparation of TEM samples by FIB. We thank the German Research Foundation (DFG) for financial support (FR 2190/4-1 Gottfried Wilhelm Leibniz Prize 2010). This work was conducted under the framework of the Research and Development Program of the Korea Institute of Energy Research (KIER) (B4-2434-01). One of us (E.Z.) thanks the Shore Research Fund in Advanced Composites (Technion) for financial support.

Supporting Information Available: POM images of crystalline $CaCO_3$ MLA showing lamellar patterns (Figure S1). Images of partially crystallized MLA taken with the aid of different light microscope techniques and showing structurally different $CaCO_3$ domains (Figures S2 and S3). Results of photolithography experiment (Figure S4) and additional TEM images (Figure S5). This material is available free of charge *via* the Internet at http://pubs.acs.org.

REFERENCES AND NOTES

1. Mann, S. *Biomineralization: Principles and Concepts in Bioinorganic Materials Chemistry*; Oxford University Press: Oxford, 2001.
2. Weiner, S.; Addadi, L. Design Strategies in Mineralized Biological Materials. *J. Mater. Chem.* **1997**, *7*, 689–702.
3. Xu, A. W.; Ma, Y. R.; Colfen, H. Biomimetic Mineralization. *J. Mater. Chem.* **2007**, *17*, 415–449.
4. Aizenberg, J.; Hendler, G. Designing Efficient Microlens Arrays: Lessons from Nature. *J. Mater. Chem.* **2004**, *14*, 2066–2072.
5. Kato, T.; Sugawara, A.; Hosoda, N. Calcium Carbonate-Organic Hybrid Materials. *Adv. Mater.* **2002**, *14*, 869–877.
6. Meldrum, F. C. Calcium Carbonate in Biomineralisation and Biomimetic Chemistry. *Int. Mater. Rev.* **2003**, *48*, 187–224.
7. Nudelman, F.; Sommerdijk, N. A. J. M. Biomineralization as an Inspiration for Materials Chemistry. *Angew. Chem., Int. Ed.* **2012**, *51*, 6582–6596.
8. Schenk, A. S.; Zlotnikov, I.; Pokroy, B.; Gierlinger, N.; Masic, A.; Zaslansky, P.; Fitch, A. N.; Paris, O.; Metzger, T. H.; Colfen, H.; *et al.* Hierarchical Calcite Crystals with Occlusions of a Simple Polyelectrolyte Mimic Complex Biomineral Structures. *Adv. Funct. Mater.* **2012**, *22*, 4668–4676.
9. Killian, C. E.; Metzler, R. A.; Gong, Y. U. T.; Olson, I. C.; Aizenberg, J.; Politi, Y.; Wilt, F. H.; Scholl, A.; Young, A.; Doran, A.; *et al.* Mechanism of Calcite Co-orientation in the Sea Urchin Tooth. *J. Am. Chem. Soc.* **2009**, *131*, 18404–18409.
10. Ma, Y.; Cohen, S. R.; Addadi, L.; Weiner, S. Sea Urchin Tooth Design: An "All-Calcite" Polycrystalline Reinforced Fiber Composite for Grinding Rocks. *Adv. Mater.* **2008**, *20*, 1555–1559.
11. Aizenberg, J.; Tkachenko, A.; Weiner, S.; Addadi, L.; Hendler, G. Calcitic Microlenses as Part of the Photoreceptor System in Brittlestars. *Nature* **2001**, *412*, 819–822.
12. Yu, K. L.; Fan, T. X.; Lou, S.; Zhang, D. Biomimetic Optical Materials: Integration of Nature's Design for Manipulation of Light. *Prog. Mater. Sci.* **2013**, *58*, 825–873.
13. Vukusic, P.; Sambles, J. R. Photonic Structures in Biology. *Nature* **2003**, *424*, 852–855.
14. Meldrum, F. C.; Colfen, H. Controlling Mineral Morphologies and Structures in Biological and Synthetic Systems. *Chem. Rev.* **2008**, *108*, 4332–4432.
15. Colfen, H. Precipitation of Carbonates: Recent Progress in Controlled Production of Complex Shapes. *Curr. Opin. Colloid Interface Sci.* **2003**, *8*, 23–31.
16. Sone, E. D.; Weiner, S.; Addadi, L. Morphology of Goethite Crystals in Developing Limpet Teeth: Assessing Biological Control over Mineral Formation. *Cryst. Growth Des.* **2005**, *5*, 2131–2138.
17. Lee, K.; Wagermaier, W.; Masic, A.; Kommareddy, K. P.; Bennet, M.; Manjubala, I.; Lee, S. W.; Park, S. B.; Colfen, H.; Fratzl, P. Self-Assembly of Amorphous Calcium Carbonate Microlens Arrays. *Nat. Commun.* **2012**, *3*, 725.
18. Sambles, R. Optics: Armed for Light Sensing. *Nature* **2001**, *412*, 783–783.
19. Chandra, D.; Yang, S.; Lin, P. C. Strain Responsive Concave and Convex Microlens Arrays. *Appl. Phys. Lett.* **2007**, *91*, 251912.
20. Yang, S.; Ullal, C. K.; Thomas, E. L.; Chen, G.; Aizenberg, J. Microlens Arrays with Integrated Pores as a Multipattern Photomask. *Appl. Phys. Lett.* **2005**, *86*, 201121.
21. Aizenberg, J.; Muller, D. A.; Grazul, J. L.; Hamann, D. R. Direct Fabrication of Large Micropatterned Single Crystals. *Science* **2003**, *299*, 1205–1208.
22. Colfen, H. Single Crystals with Complex Form via Amorphous Precursors. *Angew. Chem., Int. Ed.* **2008**, *47*, 2351–2353.
23. Li, C.; Qi, L. M. Bioinspired Fabrication of 3D Ordered Macroporous Single Crystals of Calcite from a Transient Amorphous Phase. *Angew. Chem., Int. Ed.* **2008**, *47*, 2388–2393.
24. Park, R. J.; Meldrum, F. C. Synthesis of Single Crystals of Calcite with Complex Morphologies. *Adv. Mater.* **2002**, *14*, 1167–1169.
25. Fratzl, P.; Fischer, F. D.; Svoboda, J.; Aizenberg, J. A Kinetic Model of the Transformation of a Micropatterned Amorphous Precursor into a Porous Single Crystal. *Acta Biomater.* **2010**, *6*, 1001–1005.
26. Pokroy, B.; Kapon, M.; Marin, F.; Adir, N.; Zolotoyabko, E. Protein-Induced, Previously Unidentified Twin form of Calcite. *Proc. Natl. Acad. Sci. U.S.A.* **2007**, *104*, 7337–7341.
27. Bruno, M.; Massaro, F. R.; Rubbo, M.; Prencipe, M.; Aquilano, D. (104), (018), (012), and (001) Twin Laws of Calcite ($CaCO_3$): Equilibrium Geometry of the Twin Boundary Interfaces and Twinning Energy. *Cryst. Growth Des.* **2010**, *10*, 3102–3109.
28. Jenkins, F. A.; White, H. E. *Fundamentals of Optics*, 3rd ed.; McGraw-Hill: New York, 1957.
29. Politi, Y.; Metzler, R. A.; Abrecht, M.; Gilbert, B.; Wilt, F. H.; Sagi, I.; Addadi, L.; Weiner, S.; Gilbert, P. U. P. A. Transformation Mechanism of Amorphous Calcium Carbonate into Calcite in the Sea Urchin Larval Spicule. *Proc. Natl. Acad. Sci. U.S.A.* **2008**, *105*, 17362–17366.
30. Paris, O.; Li, C. H.; Siegel, S.; Weseloh, G.; Emmerling, F.; Riesemeier, H.; Erko, A.; Fratzl, P. A New Experimental Station for Simultaneous X-Ray Microbeam Scanning for Small- and Wide-Angle Scattering and Fluorescence at BESSY II. *J. Appl. Crystallogr.* **2007**, *40*, S466–S470.